Int. J. Solids Structures Vol. 23, No. 11, pp. 1535–1549, 1987
Printed in Great Britain.

0020-7683/87 $3.00+.00

THREE- AND TWO-DIMENSIONAL STRESS FIELDS NEAR DELAMINATIONS IN LAMINATED COMPOSITE PLATES

SAILENDRA N. CHATTERJEE
Materials Sciences Corporation, Gwynedd Plaza II, Bethlehem Pike, Spring House, PA 19477, U.S.A.

(*Received* 21 *February* 1986; *in revised form* 30 *October* 1986)

Abstract—A cluster of elliptic delaminations between the layers in an infinite laminated plate is considered. The three-dimensional elasticity problem is reduced to the solution of a set of integral equations and the nature of the stress singularities along the periphery of each disbond is discussed. The procedure for obtaining the equations for two-dimensional problems is also described. Physically meaningful quantities like stress intensity factors and energy release rates obtained from numerical solutions are reported for some three- and two-dimensional problems with single delaminations between similar layers and are compared with other approximate solutions.

INTRODUCTION

Delaminations in composite laminates can exist as manufacturing defects or can be created due to various reasons, namely (i) coalescence of small voids existing at interfaces, (ii) foreign object impact, (iii) peculiar stress fields near free edges, holes, plydrops or bonded joints. Fracture mechanics based methods and crack growth laws which make use of the stress field near the periphery of a delamination are attractive tools for developing design criteria for damage tolerance and in decision-making processes of acceptance of a structural component containing an inherent flaw or repair of a part damaged in service. For this reason various studies have been reported in the literature which deal with two-dimensional stress analyses of disbonded laminates and determination of material properties like delamination fracture toughness, crack growth resistance curves, or growth laws under cyclic loading. In some of these studies[1–4] two-dimensional finite element idealizations have been employed whereas strength of materials type theories have been utilized in others[5–8]. Reduction of the two-dimensional elasticity problem to a set of integral equations and their numerical solutions have also been reported[9–11] in the literature. Three-dimensional finite element techniques[12] and lower order structural (plate) theories[11, 13] (in which the disbond is assumed to be located between two laminated plates) have been utilized for determining energy release rates along the periphery of delaminations of arbitrary geometry and elliptic shapes, respectively.

This study deals with the reduction of the three-dimensional elasticity problem of a group of elliptic delaminations in an infinite laminated plate shown in Fig. 1 to the solution of a set of integral equations for determining the displacement discontinuities across the delamination surfaces. This is performed by taking the multiple Fourier transform with respect to the spatial coordinates (x_1 and x_2) of the equilibrium equations of three-dimensional anisotropic elasticity in terms of displacements and using a stiffness formulation to relate the transforms of the tractions on the disbonded interfaces to the unknown displacement discontinuities. By taking inverse transforms of these relationships, one obtains a set of integral equations. The nature of the stress singularities is obtained by considering the dominant (singular) parts of the kernels which are shown to depend on the elastic properties of the two layers above and below each disbond.

Evaluation of the regular kernels must be performed by solving the simultaneous equations which appear in the stiffness formulation for a range of values of transform parameters and subsequent integration necessary for obtaining inverse transforms. Procedures for numerical solutions and applications to three- as well as two-dimensional problems are described.

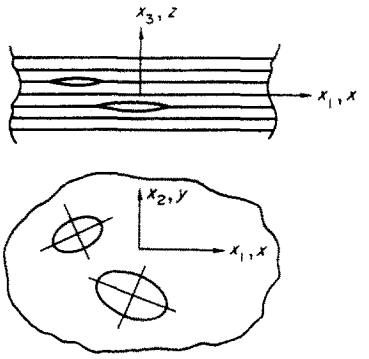

Fig. 1. Delaminations in a laminated plate.

STIFFNESS FORMULATION IN THE TRANSFORMED DOMAIN AND INTEGRAL EQUATION

The laminate (Fig. 1) is assumed to consist of a finite number of homogeneous and elastic layers, but the lateral dimensions (in x_1, x_2 directions) are considered to be infinitely large. Denoting stresses, stiffnesses and displacements by σ, C and u, respectively, the equations of three-dimensional elasticity for each layer are given by

$$\sigma_{jk,k} = 0 \tag{1}$$

$$\sigma_{jk} = C_{jklm} u_{l,m}. \tag{2}$$

Using Latin suffixes j, l which take values 1, 2, 3 and Greek suffixes α, β which take values 1, 2 substitution of eqn (2) in eqn (1) yields

$$C_{j\alpha l\beta} u_{l,\alpha\beta} + (C_{j\alpha l3} + C_{j3l\alpha}) u_{l,\alpha 3} + C_{j3l3} u_{l,33} = 0. \tag{3}$$

Taking the multiple Fourier transform with respect to x_1, x_2 of eqn (3) one obtains three ordinary differential equations in terms of the transformed displacements defined by

$$\tilde{u}_l(\xi, x_3) = \frac{1}{2\pi} \int_{-\infty}^{\infty} \int_{-\infty}^{\infty} u_l(\mathbf{x}, x_3)\, e^{i\mathbf{x}\cdot\xi}\, dx_1\, dx_2 \tag{4}$$

where $\mathbf{x} = (x_1, x_2)$ and $\xi = (\xi_1, \xi_2)$ are vectors, and $i = \sqrt{-1}$.

After determination of the characteristic roots of these equations and evaluation of the unknown constants in terms of transformed displacements on the surfaces $z = \pm h/2$ of the layer, it is possible to evaluate the stiffness matrices relating the transforms of tractions and displacements on the two surfaces. Let $[\tilde{t}_1, \tilde{t}_2, i\tilde{t}_3]^{tr}$ at $z = h/2$ be denoted as $\tilde{\mathbf{T}}_1$, where t_1, t_2 and t_3 are tractions in the positive x_1-, x_2-, and x_3-directions and $[\tilde{u}_1, \tilde{u}_2, i\tilde{u}_3]^{tr}$ at $z = h/2$ be expressed as $\tilde{\mathbf{U}}_1$. Let the corresponding quantities at $z = -h/2$ be written as $\tilde{\mathbf{T}}_2$ and $\tilde{\mathbf{U}}_2$, respectively. Then one can write

$$\begin{aligned} \tilde{\mathbf{T}}_1 &= \overset{11}{[K]}\tilde{\mathbf{U}}_1 + \overset{12}{[K]}\tilde{\mathbf{U}}_2 \\ \tilde{\mathbf{T}}_2 &= \overset{21}{[K]}\tilde{\mathbf{U}}_1 + \overset{22}{[K]}\tilde{\mathbf{U}}_2 \end{aligned} \tag{5}$$

where $\overset{21}{[K]} = \overset{12}{[K]}^{tr}$. Calculation of stiffness matrices for isotropic layers is straightforward. Closed form expressions for transversely isotropic layers when the normal to the plane of isotropy is parallel to the x_1–x_2 plane are given in Appendix A. Commonly used unidirectional fiber composites fall in this category.

Introducing the transforms of displacement discontinuities $\tilde{\mathbf{v}}_j^*$ across the jth delaminated surface as unknowns and making use of a global stiffness formulation described in

Appendix B, it is possible to express the transforms of tractions $\bar{\mathbf{T}}_j^*$ on the top face of layer l_j below the disbond in terms of $\mathbf{v}_j^*$ (eqn (B8)). Denoting $\mathbf{T}_j^r(\mathbf{x})$ and $\mathbf{v}_j^r(\mathbf{x})$ as the prescribed tractions on the bottom face of disbond r on the jth surface and the displacement discontinuity across the same delaminated area, respectively. Taking the inverse transform of eqn (B8) one obtains the following equations for m disbonded interfaces, jth interface containing Q_j numbers of disbonds:

$$\mathbf{T}_j^r(\mathbf{x}') = \sum_{p=1}^{m} \sum_{q=1}^{Q_p} \int [G_{jp}^{rq}(\mathbf{x}', \mathbf{x})] \mathbf{v}_p^q(\mathbf{x})\, \mathrm{d}A_{pq} + \overset{0}{\mathbf{T}}{}_j^r(\mathbf{x}');$$

$$\mathbf{x}' \text{ in } A_{jr} \quad r = 1, \ldots, Q_j \quad j = 1, \ldots, m \tag{6}$$

where $\overset{0}{\mathbf{T}}{}_j^r(\mathbf{x}')$ depends on the prescribed tractions on the top and bottom surfaces of the laminate, $\mathbf{x}' = (x_1', x_2')$, and each of the displacement and traction vectors contain three components in the x_1, x_2, x_3 directions. The kernels G (3×3 matrices) are given by

$$[G_{jp}^{rq}] = \frac{1}{4\pi^2} \int_{-\infty}^{\infty} \int_{-\infty}^{\infty} \xi[H^{jp}(\boldsymbol{\xi})]\, \mathrm{e}^{\mathrm{i}(\mathbf{x}-\mathbf{x}')\cdot\boldsymbol{\xi}}\, \mathrm{d}\xi_1\, \mathrm{d}\xi_2; \quad \mathbf{x}' \text{ in } A_{jr}, \mathbf{x} \text{ in } A_{pq} \tag{7}$$

$$\xi[H^{jp}] = [C^{*p}]\delta_{jp} + [C^{jp}] \tag{8}$$

$$\xi = \sqrt{(\xi_1^2 + \xi_2^2)}$$

$$\boldsymbol{\xi} = (\xi_1, \xi_2) = (\xi \cos\phi, \xi \sin\phi). \tag{9}$$

C^{*p} and C^{jp} can be evaluated in terms of ξ and ϕ by the methods described in Appendix B. δ_{jp} is the Kronecker delta.

TYPES OF STRESS SINGULARITIES

The dominant parts of the kernels are obtained by taking the effects of displacement discontinuities at one disbond on the tractions at the same place (i.e. $p = j$, $q = r$) and retaining only $[C^{*j}]$ in $\xi[H^{jp}]$ given by eqn (8). Considering only this dominant part, assuming that the principal axes of the elliptic disbond with semiaxes (a_1, a_2) coincide with x_1, x_2 axes and transforming the ellipse onto a unit circle A_0 one obtains three integral equations for determining three displacement discontinuity functions. Willis[14] discussed this problem when $a_1 = a_2$ (i.e. the case of a circle) by the use of Radon transform and his results indicate that each of the three displacement discontinuities between two different materials can be expressed as a sum of three functions, the asymptotic of which forms as the disbond periphery is approached, are given by $b_0(\theta)(1-R^2)^{1/2}$, $b_1(\theta)(1-R^2)^{1/2+\mathrm{i}\varepsilon(\theta)}$ and $\bar{b}_1(\theta)(1-R^2)^{1/2-\mathrm{i}\varepsilon(\theta)}$, (R, θ) being the polar coordinates in circle A_0, b_0, b_1, $\bar{b}_1$ are functions of θ only. Stresses near but ahead of the disbond periphery can be expressed as a sum of three functions which are similar to those for displacements with 1/2 replaced by $-1/2$. For different isotropic layers above and below the disbond ε is independent of θ. Similar stress singularities have been found to occur in two-dimensional problems of interface cracks between two dissimilar isotropic or anisotropic media[10, 15–17]. It can be shown that for the case of two anisotropic media $\varepsilon(\theta^*)$ in the three-dimensional problem coincides with ε for the two-dimensional problem when the x_1-axis is taken to coincide with the direction of the normal to the circle at $\theta = \theta^*$ and all quantities are assumed to be independent of the x_2-axis (tangent to the circle).

For the case of elliptic disbonds, following procedures similar to those used by Willis, but retaining the expression for C^* which is dependent on a_1 and a_2 (see discussions at the end of Appendix B), it is possible to show that similar stress singularities do appear where ε varies along the periphery of the disbond and is again given by the value for the two-dimensional problem with the x_1-axis coinciding with the direction normal to the ellipse at

any particular point on the disbond periphery. A physically unrealistic interpenetration associated with such singularities has been the subject of many investigations[16], dealing with two-dimensional problems. However, this will not be addressed here since in what follows we will restrict ourselves only to the case of inverse square root type singularities. It should also be noted that in many cases such interpenetration occurs over a very small zone and does not influence physically meaningful quantities like energy release rates[14, 16].

SOLUTION FOR A CLASS OF THREE-DIMENSIONAL PROBLEMS

For the purpose of numerical solution, it is necessary to express the displacement discontinuities in terms of three unknown functions which can be expanded in terms of orthogonal sets with weight functions similar to the asymptotic forms described earlier. Using similar expansion schemes for the tractions, the set of integral equations, eqns (6) and (7), can then be reduced to a system of algebraic equations. Although the asymptotic forms of the displacement discontinuities are quite clear, no expansion scheme with appropriate orthogonal sets has yet been developed for solution of the general three-dimensional problem. Willis[14] used an expansion scheme for the Radon transforms of the displacement discontinuities when ε is independent of θ. From this work and those on two-dimensional problems it is clear that considerable computational effort is necessary for solving the general problem even if appropriate orthogonal sets with ε varying along the disbond peripheries are obtained. We, therefore, defer the solution of the general problem to future studies and restrict ourselves to the case of laminates with arbitrary lamination sequence but containing delaminations only between two similar layers. For this restricted class of problems $\varepsilon = 0$ and the stress singularities are of the inverse square root type.

We now use the following transformations for $\mathbf{x}$ varying over area A_{pq} which is assumed to be elliptic in shape

$$\mathbf{x} = \overset{pq}{\mathbf{x}}{}^{0} + \overset{pq}{\mathbf{x}}{}^{1} \tag{10a}$$

where omitting the superscripts pq for the particular disbond, $\mathbf{x}^0$ is the coordinate of the center of the ellipse and

$$\mathbf{x}^{1r} = y[\cos\theta \ \sin\theta]\begin{bmatrix} a_1\cos\theta_0 & a_1\sin\theta_0 \\ -a_2\sin\theta_0 & a_2\cos\theta_0 \end{bmatrix}; \quad 0 \leqslant y \leqslant 1,\ 0 \leqslant \theta < 2\pi \tag{10b}$$

(a_1, a_2) and θ_0 being the semiaxes of the ellipse pq and the inclination of semiaxis a_1 with the x_1-axis. Use of eqns (10) yields

$$(\mathbf{x}-\mathbf{x}')\cdot\boldsymbol{\xi} = \xi y \overset{pq}{f}\cos(\theta - \overset{pq}{\eta}) - \xi y' \overset{jr}{f}\cos(\theta' - \overset{jr}{\eta}) + \xi R_0\cos(\phi-\phi_0)$$

where

$$\overset{pq}{f}(\phi) = \sqrt{(a_1^2\cos^2(\phi-\theta_0) + a_2^2\sin^2(\phi-\theta_0))}$$

$$\overset{pq}{\eta}(\phi) = \tan^{-1}\left(\frac{a_2}{a_1}\tan(\phi-\theta_0)\right) \tag{11a-c}$$

R_0 is the projection of the line segment joining the center of the ellipse jr to that of pq on the x_1–x_2 plane and ϕ_0 is the angle which this projected line makes with the x_1-axis. Relations similar to eqns (11b) and (11c) hold for $\overset{jr}{f}(\phi)$ and $\overset{jr}{\eta}$. In what follows we will omit the superscripts pq and jr and denote $\overset{pq}{f}, \overset{pq}{\eta}, \overset{jr}{f}, \overset{jr}{\eta}$ by f, η, f', η', respectively, all of which are functions of ϕ. With these notations one can write[18]

$$e^{i\xi yf\cos(\theta-\eta)} = J_0(\xi fy)+2\sum_{s=1}^{\infty}(i)^s J_s(\xi fy)\cos s(\theta-\eta) \tag{12}$$

and a similar series with i replaced by $-i$ for $\exp[-i\xi y'f'\cos(\theta-\eta')]$, J_s being the Bessel functions of the first kind of order s. We can now expand each of the three components of the vector functions $v_p^{q^*}$ $(=V_\partial^*, \partial = 1,2,3)$ and $T_j^{r^*} - \overset{0}{T}{}_j^r$ $(= t_\gamma, \gamma = 1,2,3)$ as

$$V_\delta^*(\mathbf{x}) = \sum_{s=0}^{\infty}\sum_{\beta=1}^{4} y^{s_{\beta\delta}} V^{\beta}_{\delta s_{\beta\delta}}(y)\psi_{s_{\beta\delta}}(\theta)$$

$$t_\gamma(\mathbf{x}') = \sum_{s=0}^{\infty}\sum_{\alpha=1}^{4} a_0(s'_{\alpha\gamma})\, t^{\alpha}_{\gamma s'_{\alpha\gamma}}(y')\psi_{s'_{\alpha\gamma}}(\theta')$$

$$\psi_{s_{\beta\delta}}(\theta) = \cos s_{\beta\delta}\theta; \quad \beta = 1,3 \qquad a_0 = 1; \quad s'_{\alpha\gamma} = 0$$
$$= \sin s_{\beta\delta}\theta; \quad \beta = 2,4 \qquad = 2; \quad s'_{\alpha\gamma} > 0$$

$$s_{\beta\delta} = 2s \quad \text{for } \beta = 1,2, \delta = 1,2 \quad \text{and } \beta = 3,4, \delta = 3$$
$$= 2s+1 \quad \beta = 3,4, \delta = 1,2 \quad \text{and } \beta = 1,2, \delta = 3. \tag{13}$$

Expanding $V^{\beta}_{\delta s_{\beta\delta}}$ in a series of Jacobi polynomials

$$V^{\beta}_{\delta s_{\beta\delta}} = \sum_{n=1}^{\infty} v^{\beta n}_{\delta s_{\beta\delta}}(1-y^2)^{1/2} P_{n-1}^{(1/2, s_{\beta\delta})}(2y^2-1) \tag{14}$$

and using the identity

$$P_{n-1}^{(1/2,s)}(2y^2-1) = \sum_{n_1=1}^{n} d^s_{n_1 n}(1-y^2)^{n_1-1} \tag{15}$$

where

$$d^s_{1n} = \Gamma(n+\tfrac{1}{2})/[(n-1)!\,\Gamma(3/2)]$$
$$d^s_{(n_1+1)n}/d^s_{n_1 n} = (n+s+\tfrac{1}{2}+n_1-1)(n_1-n)/[(3/2+n_1-1)n_1]$$

and Γ denotes the gamma function, which is obtained by using the expression of Jacobi polynomials in terms of the hypergeometric function, and other integral formulae[18], one can write

$$t^{r\alpha}_{js'_{\alpha\gamma}}(y') = \sum_p\sum_q\sum_{\beta=1}^{4}\sum_{\partial=1}^{3}\sum_s\sum_n L^{op\partial s_{\beta\delta} r\alpha}_{js'_{\alpha\gamma} q\beta n}(y') v^{q\beta n}_{p\partial s_{\beta\delta}} \tag{16}$$

for $s' = 0, 1, \ldots, \infty$ and the range of values of j, r, α, and γ given earlier. In the right-hand side sums over p and q are as in eqn (6) and those over s, n denote the infinite series, eqns (13) and (14). $s_{\beta\delta}$ and $s'_{\alpha\gamma}$ are given in eqns (13), and

$$L^0 = \frac{a_1 a_2}{\pi}(-1)^{s+s'}\sum_{n_1=1}^{n}\int_0^{\pi}\int_0^{\infty}(f)^{-1/2-n_1} d^{s_{\beta\delta}}_{n_1 n} e_{n_1}\psi_{s_{\beta\delta}}(\eta)\psi_{s_{\alpha\gamma}}(\eta') H^{j\beta}_{\gamma\delta}(\xi,\phi) H'^{\alpha\beta}_{\gamma\delta}(\xi,\phi,R_0,\phi_0)$$
$$\times J_{s_{\beta\delta}+n_1+1/2}(\xi f)\xi^{3/2-n_1} J_{s'_{\alpha\gamma}}(\xi f' y')\,\mathrm{d}\xi\,\mathrm{d}\phi \tag{17}$$

$$e_{n_1} = 2^{n_1-1/2}\Gamma(n_1+\tfrac{1}{2})$$

a_1, a_2 are the semiaxes of the elliptic disbond pq, and $H'^{\alpha\beta}$ ($\alpha = 1, 2, \ldots, 4$; $\beta = 1, 2, \ldots, 4$) are 3×3 matrices given below.

For $\alpha\beta = 1, 2$

$$H' = C_1 \begin{bmatrix} 1 & 1 & -1 \\ 1 & 1 & -1 \\ -1 & -1 & 1 \end{bmatrix}. \tag{18}$$

For $\alpha\beta = 3, 4$ the multiplier remains the same as C_1 but all the elements of the matrix are equal to 1. For $\alpha = 1, 2$; $\beta = 3, 4$ the multiplier is S_1; the elements of the first two rows are equal to -1 and the others are equal to 1. For $\alpha = 3, 4$; $\beta = 1, 2$ the multiplier is again S_1 but the elements of the first two columns are equal to 1 and the others are equal to -1. C_1 and S_1 are given by

$$C_1 = \cos\{\xi R_0 \cos(\phi - \phi_0)\}, \qquad S_1 = \sin\{\xi R_0 \cos(\phi - \phi_0)\}.$$

R_0 and ϕ_0 are defined in the statements after eqn (11). Note that we have used the properties $H_{\gamma\delta}(\pi + \phi) = H_{\gamma\partial}(\phi)$, $\gamma\partial = 11, 12, 22, 21, 33$ and $H_{\gamma\partial}(\pi + \phi) = -H_{\gamma\partial}(\phi)$, $\gamma\partial = 13, 31, 23, 32$. Note that the coupling between delaminations vanish when $R_0 \to \infty$ by virtue of the Riemann–Lebsesgue lemma. Also, some of the displacement components become uncoupled when $R_0 = 0$.

Multiplying both sides of eqn (15) by $y'^{s'_{\alpha\gamma}+1}(1-y'^2)^{1/2} P_{n'-1}^{(1/2, s'_{\alpha\gamma})}$ ($n' = 1, 2, \ldots$) and integrating with respect to y' from 0 to 1 one obtains the following set of algebraic equations:

$$t^{r\alpha n'}_{j\gamma s'_{\alpha\gamma}} = \sum_{p=1}^{m} \sum_{q=1}^{Q_p} \sum_{\beta=1}^{4} \sum_{\partial=1}^{3} \sum_{s=0}^{\infty} \sum_{n=1}^{\infty} L^{p\partial s_{\beta\delta} r\alpha n'}_{j\gamma s'_{\alpha\gamma} q\beta n} v^{q\beta n}_{p\partial s_{\beta\partial}} \tag{19}$$

$$j = 1, \ldots, m; \; r = 1, \ldots, Q_j; \quad \alpha = 1, \ldots, 4, \gamma = 1, \ldots, 3; \; s' = 0, 1, \ldots, \infty; \; n' = 1, \ldots, \infty$$

where L is given by an expression similar to that for L^0 in eqn (17) with a summation over n'_1 from 1 to n' and the terms $\xi^{3/2-n_1} J_{s'_{\alpha\gamma}}(\xi f' y)$ replaced by

$$\xi^{1-n-n'_1} J_{s'_{\alpha\gamma}+n'_1+1/2}(\xi f')\, d^{s'_{\alpha\gamma}}_{n'_1 n'} e_{n'_1}.$$

Truncating the system and retaining terms such that $s, s' \leqslant s_{\max}$ and $n \leqslant N(s)$, $n' \leqslant N(s')$, where $N(s) = s_{\max} - s + 1$, one can obtain an approximate solution of the system. Noting that $[C^{*p}]$ in eqn (3) can be written as $\xi[C^{op}(\phi)]$, and $H^{\alpha\gamma}_{\gamma\delta} = 1, -1$ or 0 when $j = p$, $r = q$ the integral with respect to ξ for the dominant part of the kernel can be explicitly evaluated with the help of formulae[18]. Other integrals with respect to ξ and ϕ are evaluated numerically. In this study we have used the trapezoidal rule for integration with respect to ϕ (with conditions $F(\xi, \pi) = F(\xi, 0)$) and used the transformation $\xi = (\xi^*\zeta)/(1-\zeta)$ to transform the domain $(0 < \xi < \infty)$ to $(0 < \zeta < 1)$ along with Simpson's rule to perform the integration with respect to ζ (with the conditions $F(0, \phi) = F(\infty, \phi) = 0$). A value of $S_{\max} = 3$, ten integration points for ϕ and 80 points for ζ (equally spaced) with $\xi^* = 80$ were found to yield reasonably accurate results in the problems discussed later.

STRESS INTENSITY FACTORS AND ENERGY RELEASE RATES

To evaluate the stress intensity factors, we make use of eqns (16) and (17) and restrict our attention to the region y' greater than but in the neighborhood of 1. We retain only the dominant part $[C^{op}(\phi)] = 1/\xi[C^{*p}]$ of $[H^{jp}]$ and the terms for $p = j$ and $q = r$ (i.e. v^q_p for the

same disbond where stresses are being evaluated). It can be shown that the interactive traction imposed by the layer above the jth interface on the layer below is bounded except for $n_1 = 1$.

After some algebraic manipulations, the tractions can be expressed as ($\gamma = 1, 2, 3$)

$$t_\gamma(\eta) \approx (y'-1)^{-1/2} \sum_\beta \sum_\delta \sum_s \sum_n L^{**}(\eta) \psi_{s_{\beta\delta}}(\eta) v^{\beta n}_{\partial s_{\beta\partial}}$$

where

$$L^{**}(\eta) = Ag(\eta) f(\phi)^{-3} C^{\alpha\beta}_{\gamma\delta}(\phi)$$

$$A = -a_1 a_2 2^{1/2} [\Gamma(\tfrac{1}{2})\Gamma(n+\tfrac{1}{2})]/[\pi(n-1)!]$$

$$\phi = \tan^{-1}\left(\frac{a_1 \tan\eta}{a_2}\right) + \theta_0$$

$$g(\eta) = \left(\frac{\cos^2\eta}{a_1^2} + \frac{\sin^2\eta}{a_2^2}\right). \tag{20a–e}$$

The sum over δ is evaluated over 1, 2 for $\gamma = 1, 2$, and for $\gamma = 3$, $\delta = 3$ is taken.

Asymptotic forms of the displacement discontinuities are given by

$$V_\delta(\eta) \approx 2(1-y)^{1/2} \sum_\beta \sum_s \sum_n \psi_{s_{\beta\delta}}(\eta) v^{\beta n}_{\delta s_{\beta\delta}} \frac{\Gamma(n+\frac{1}{2})}{(n-1)!}. \tag{21}$$

If R, R' are the distances measured in the direction of the outward and inward normal to the elliptic disbond one can write

$$(y'-1)^{1/2} = R^{-1/2}/(g(\eta))^{1/4} \quad y' > 1$$

and (22)

$$(1-y)^{1/2} = R'^{1/2}(g(\eta))^{1/4} \qquad y < 1.$$

The stress intensity factors for modes II and III can be calculated by taking the components of t_1 and t_2 in the directions normal and tangential to the disbond periphery and multiplying the sum appearing in the right-hand side of eqn (20a) by $(g(n))^{1/4}$. For mode I the sum (with $\partial = 3$ only) is multiplied by the same factor. For calculation of the mode I component of the energy release rate the concept of work done for crack closure (due to Irwin) can be directly utilized. For modes II and III it is necessary to calculate the discontinuities in displacements normal and tangential to the disbond periphery which can be evaluated from eqn (21). The details are straightforward and omitted for brevity.

TWO-DIMENSIONAL PROBLEMS

For two- (or quasi-three) dimensional problems where the elliptic delaminations are replaced by disbonds which are infinitely long in the x_2 direction, all quantities can be assumed to be independent of x_2. In such problems the vectors $\mathbf{x}'$ and $\mathbf{x}$ are to be replaced by x_1' and x_1, respectively, in the integral equation, eqn (6), and the integral is taken over the length of each delamination in the x_1 direction. The kernel in eqn (7) is evaluated by integrating with respect ξ_1 only (since only the single Fourier transform is required) and ξ_2 everywhere else (in eqns (7)–(9)) is taken equal to zero. Solution of such singular integral equations and resulting stress singularities has been considered in several studies[9, 10, 17]. For delaminations between similar layers the dominant kernels are Cauchy kernels and stress singularities are of the inverse square root type. Collocation methods and Gauss–

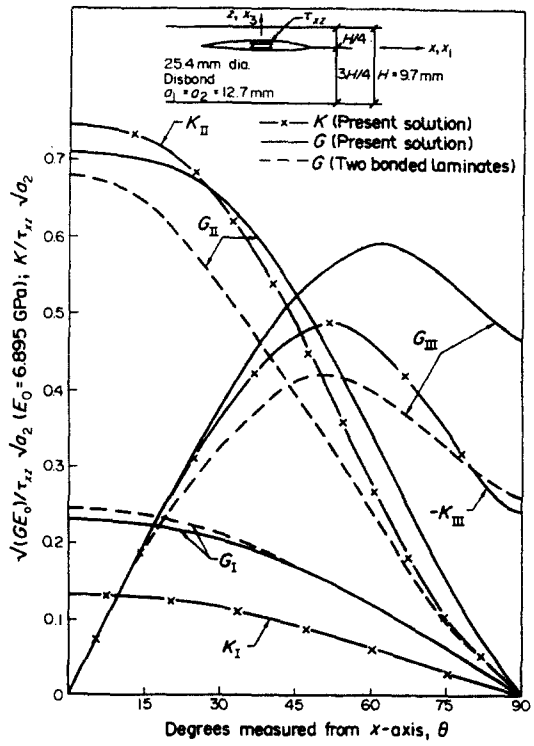

Fig. 2. Intensity factors and energy release rates in a $((0_4/+45_2)_s)_4$ laminate for a quarter plane disbond under xz shear.

Chebyshev integration formula[19] are utilized to obtain the results for two-dimensional problems reported later. Numerical integration is utilized to evaluate the regular kernels.

RESULTS, APPLICATIONS AND DISCUSSIONS

Variation of strain energy release rates and stress intensity factors along the periphery of a 25.4 mm diameter circular disbond located at the quarter plane of a $((0_4/\pm 45_2)_s)_4$ AS1/3501-6 laminate due to transverse shear stress applied on disbond surfaces is shown in Fig. 2. The 0° lamina properties (ply thickness = 0.1514 mm) used for calculations are Young's moduli $E_A = 125$ GPa, $E_T = 10$ GPa; Poisson's ratio $\nu_A = 0.28$ (transverse strain for unit axial strain) and shear moduli $G_A = 5.8$ GPa, $G_T = 3.7$ GPa, A and T denoting axial and transverse properties. Results are plotted against angle θ (from the x-axis) from 0° to 90° since for all practical purposes the intensity factors are antisymmetric about the y-axis and symmetric about the x-axis. Also plotted in Fig. 2 are the energy release rates obtained from the approximate bonded plate model[11, 13]. The results are in close agreement with the present solution especially in the case of G_{II} and G_I, possibly because the plate bending rigidities D_{11} of the two plates are extremely high as compared to shear stiffnesses. D_{22} and D_{66} are not as large as D_{11} (see Ref. [11]) and possibly for that reason there is more discrepancy in the values of G_{III} for $\theta > 45°$. Similar comparisons can be found elsewhere[20] for a midplane disbond where the differences are less than those in Fig. 2.

Therefore, failure loads for quasi-static fracture of test specimens with midplane disbonds obtained from the present solution will be close to those obtained from the bonded plate model as well as experimental data[13, 20].

Results for a midplane disbond (45.8 mm diameter) in a $((30_4/(75/-15)_2)_s)_4$ laminate of the same material with a ply thickness of 0.1328 mm ($E_A = 142$ GPa, other properties chosen to be the same as in the problem described above) with prescribed shears on the disbond surfaces are plotted in Fig. 3 for $\tau_{xz}/\tau_{yz} = 5.4$. This ratio is the value which will be found in a laminate carrying a shear force Q_x with all quantities independent of the y-coordinate. The results are interesting in the fact that at some points G_{II} (or G_{III}) are

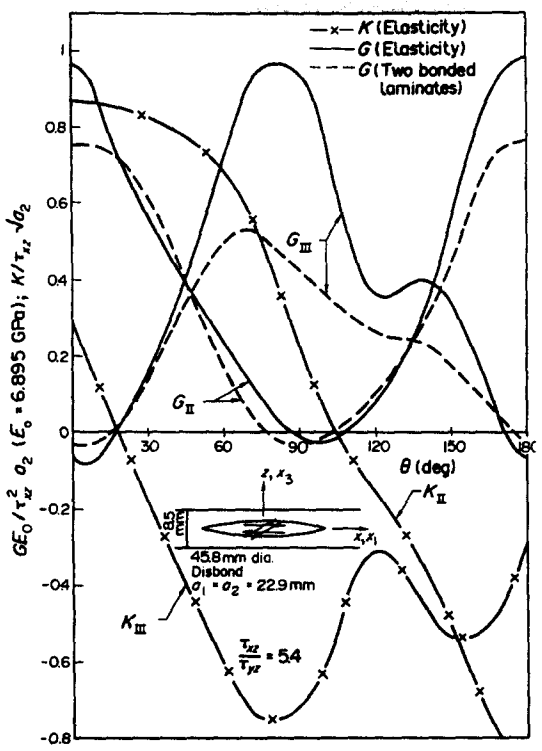

Fig. 3. Intensity factors and energy release rates in a $((30_4/(75/-15)_2)_s)_4$ laminate for a midplane disbond under xz and yz shear.

negative although the total energy release rate at every point is always positive. This phenomenon has no counterpart in problems of isotropic media since the energy release rate components I, II, III are related to the squares of the corresponding intensity factors. Individual components of the energy release rates or their sum are often used for calculating quasi-static fracture load and growth of such disbonds under fatigue[11–13]. Although the phenomenon discussed above may not affect quasi-static fracture loads, it may have some influence on the growth of disbonds under fatigue if it is assumed that the rate of growth per cycle depends on the stress field ahead of but near to the disbond periphery (in metals this influences the plastic zone size). Therefore, a scalar function of the intensity factors or its range under fatigue loading may be better suited for quantitative correlation with crack growth rate. Such a model has been used extensively in a detailed experimental/analytical correlation study[20] with single as well as multiple elliptic disbonds in various laminate configurations. Results given in Fig. 3 are for $0 \leqslant \theta \leqslant \pi$ and $K(\pi+\theta) = -K(\theta)$. Energy release rates obtained from the bonded plate model[11, 13] plotted in the same figure show significant differences in the values of G_{III}, possibly for the same reasons discussed in the previous paragraph.

Figures 4 and 5 show the displacement discontinuity gradients for the plane strain problem of a 25.4 mm long midplane disbond in a $((0_4/\pm 45_2)_s)_4$ laminate subjected to tractions in the x and z directions, respectively, equal and opposite on the two faces. For the finite element results we have made use of constant strain triangular elements which yields finite values of the gradients at the crack tips in contrast to the square root singularities in the elasticity solution. In both solutions we have replaced the (± 45) layers by a material with smeared properties based on the assumption of constant in-plane strains and constant transverse shear and normal stresses. This was done to limit the number of degrees of freedom in the finite element model where layers of different orientations have to be modelled separately. Each ply is assumed to be 0.1398 mm thick. The 0° layers are assumed to have an axial Young's modulus E_A of 125 GPa and other properties the same as those in the two previous problems. Although the singularity at the tips is not strictly modelled in the finite element solution the displacement gradient is very accurately predicted elsewhere.

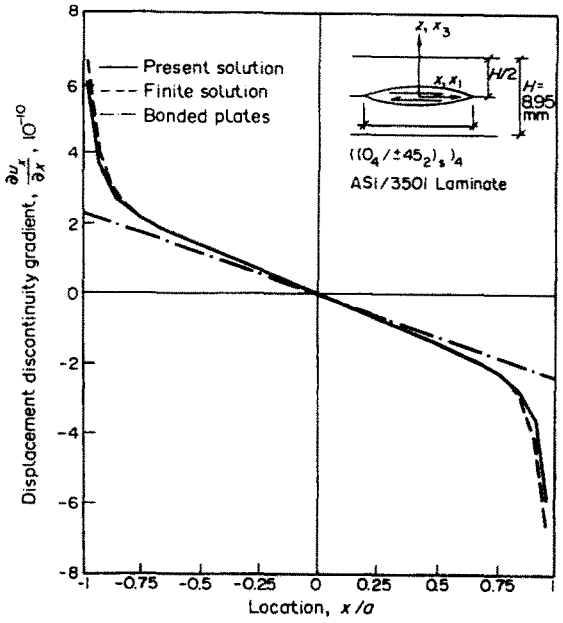

Fig. 4. Displacement discontinuity gradient for unit shear stress, plane strain.

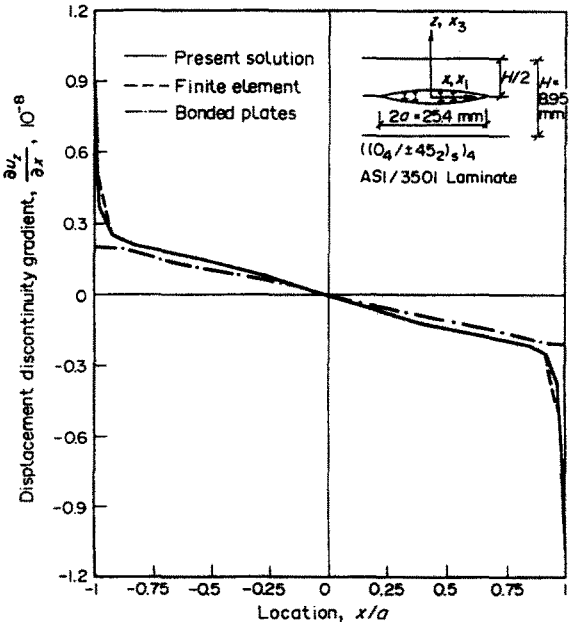

Fig. 5. Displacement discontinuity gradient for unit normal stress, plane strain.

Elements with singular fields or other modifications may be utilized to obtain more accurate results. However, for the present work such modifications are not attempted since the energy release rates were found to be quite accurate. Also shown in the figures are two approximate closed form solutions, where the disbond is assumed to be located between two laminated plates which behave according to shear deformation plate theory but are subjected to unknown tractions on bonded parts of the interface. These are two-dimensional versions of the bonded plate model[11, 13] and the solutions are given in Appendix C. Although the results show significant differences in the displacement gradient from the other two solutions near the tips, energy release rates computed are not far off from those obtained from elasticity and finite element solutions as given in Table 1.

These results are not surprising since strength of materials type solutions are known to yield a good measure of energy release rates in many problems without the capability to model the exact deformation patterns near crack tips. For the same reason the bonded

Table 1. Non-dimensionalized energy release rates for midplane disbonds in $((0_4/\pm 45_2)_s)_4$ laminates under plane strain $E_0 = 6.895$ GPa, $2a = 25.4$ mm

	Disbond under unit shear stress $\sqrt{\left(\frac{G_{II}E_0}{2a}\right)}$	Disbond under unit normal stress $\sqrt{\left(\frac{G_I E_0}{2a}\right)}$
Present	0.77	2.48
Finite element	0.73	2.39
Close form solution	0.64	2.24

plate model yields results close to elasticity solutions for the three-dimensional problems considered. Double cantilever beam specimens commonly used for mode I fracture characterization[6] are usually analyzed by such strength of materials type solutions. In the results given in Table 1, the difference in $\sqrt{G_I}$ in the mode I problem is 10%. Whereas that in $\sqrt{G_{II}}$ for the mode II case is about 16%. These differences usually depend on the ratio of disbond length to the plate thicknesses and should become less if these ratios are increased. Therefore, some care should be taken in using such elementary solutions for material characterization studies.

In calculating the energy release rates from the finite element solutions we have made use of the same principles as in the bonded plate models by taking half of the product of the interactive nodal force acting on the top half at the tip node and the displacement discontinuity gradient evaluated from the element above and below the disbonds closest to the tip.

It may not be necessary to use finite elements with singular fields to obtain accurate values of energy release rates. It should be pointed out, however, that in problems where the disbond is not on the midplane mixed mode effects will exist and the displacement discontinuities will be such that the disbond may remain partially closed. Also the relative influence of each mode on fracture is not very clear. Although attempts have been made in the past to predict fracture using the total energy rates without any consideration to such closures under mixed mode conditions and the results are found to be close to test data (see Ref. [11], where elasticity solutions have been utilized), further studies should be conducted to determine the sensitivity of results to the closure effects as well as different mixed mode fracture criteria.

In all applications considered here we have assumed that disbond growth will be coplanar and indeed in many cases such a growth pattern may cause failure. There are, however, examples[11, 13, 20] where non-coplanar growth can occur, i.e. when the disbond can find easy paths to grow without cutting across fibers. It is hoped future studies will be directed at modelling such growth to obtain a better understanding of this interesting but complicated subject of delamination fracture.

Acknowledgements—The author expresses his sincere appreciation to the Naval Air Development Center, Warminster, Pennsylvania, for sponsoring this work under contract No. N62269-82-C-0705. Thanks are due to Mr V. Ramnath for his help in obtaining some of the numerical results.

REFERENCES

1. E. F. Rybicki, D. W. Schmueser and J. Fox, An energy release rate approach for stable crack growth in the free edge delamination problem. *J. Composite Mater.* **11**, 470–487 (1977).
2. S. S. Wang, An analysis of delamination in angle-ply fiber reinforced composites. *ASME J. Appl. Mech.* **47**, 64–70 (1980).
3. A. S. D. Wang and F. W. Crossman, Initiation and growth of transverse cracks and edge delaminations in composite laminates. *J. Composite Mater.* 71–106 (Supplemental Vol. 1980).
4. G. E. Law, A mixed mode fracture analysis of $(\pm 25/90_n)_s$ graphite/epoxy composite laminates. In *Effects of Defects in Composite Materials*, ASTM STP 836, pp. 143–160. American Society of Testing of Materials (1984).
5. D. F. Devitt, R. A. Schapery and W. L. Bradley, A method of determining the mode I fracture toughness of elastic and viscoelastic composites. *J. Composite Mater.* **14**, 270–285 (1980).

6. F. X. DeCharentenay, J. M. Harry, N. J. Prel and M. L. Benzeggah, Characterizing the effect of delamination defect by mode I delamination test. In *Effects of Defects in Composite Materials*, ASTM STP 836, pp. 84–103. American Society of Testing of Materials (1984).
7. T. K. Obrien, Mixed mode strain energy release rate effects on edge delamination in composites. In *Effects of Defects in Composite Laminates*, ASTM STP 836, pp. 125–142. American Society of Testing of Materials (1984).
8. R. L. Ramkumar, S. V. Kulkarni, R. B. Pipes and S. N. Chatterjee, Analytical modeling and ND monitoring of interlaminar defects in fiber reinforced composites. In *Fracture Mechanics, Proceedings of the Eleventh Symposium on Fracture Mechanics*, Pennsylvania, 1, ASTM STP 677, pp. 668–684. American Society of Testing of Materials (1979).
9. S. N. Chatterjee, On interlaminar defects in laminated composites. In *Modern Developments in Composite Materials and Structures*, pp. 1–15. ASME (1979).
10. S. N. Chatterjee, M. J. Pindera, R. B. Pipes and W. A. Dick, Composite defect significance, Naval Air Development Center Contracts Reports, NADC 81034-60, Warminster, PA, 18974, pp. 92–106 (November 1982).
11. S. N. Chatterjee, R. B. Pipes and R. A. Blake, Jr., Criticality of disbonds in laminated composites. In *Effects of Defects in Composite Materials*, ASTM STP 836, pp. 161–174. American Society of Testing of Materials (1984).
S. N. Chatterjee and R. B. Pipes, Composite defect significance, Naval Air Development Center Contract Report, NADC 80048-60 (August 1981).
12. D. J. Wilkins, J. R. Eisenman, R. A. Camin, W. S. Margolis and R. A. Benson, Characterizing delamination growth in graphite–epoxy. In *Damage in Composite Materials: Basic Mechanisms, Accumulation, Tolerance and Characterization*, ASTM STP 775, pp. 162–183. American Society of Testing of Materials (1982).
13. S. N. Chatterjee, R. B. Pipes and W. A. Dick, Mixed mode delamination fracture in laminated composites. *Composites Sci. Technol.* **25**(1), 49–67 (1986).
14. J. R. Willis, The penny shaped crack on an interface. *Q. J. Mech. Appl. Math.* **XXV**(3), 367–385 (1972).
15. A. H. England, A crack between dissimilar media. *ASME J. Appl. Mech.* **32**, 400–402 (1965).
16. S. S. Wang and I. Choi, The interface crack between dissimilar anisotropic composite materials. *ASME J. Appl. Mech.* **50**, 169–178 (1983). Also, see M. Comminon, The interface crack. *ASME J. Appl. Mech.* **45**, 631–636 (1977).
17. F. Erdogan, Approximate solutions of singular integral equations. *SIAM J. Appl. Math.* **17**, 1041–1059 (1969).
18. I. S. Gradshteyn and I. M. Ryzhik, *Tables of Integrals Series and Products*. Academic Press, New York (1965).
19. F. Erdogan, G. D. Gupta and T. S. Cook, Numerical solution of singular integral equations. In *Methods of Analysis and Solutions to Crack Problems* (Edited by G. C. Sih), Chap. 7. Wolters Noordhoff (1972).
20. S. N. Chatterjee, V. Ramnath, W. A. Dick and R. B. Pipes, Composite defect significance, Naval Air Development Center, Final Report (Draft), NADC Contract No. N62269-82-C-0705 (February 1985).

APPENDIX A. STIFFNESS MATRICES OF TRANSVERSELY ISOTROPIC LAYERS

In fiber composite laminates commonly used in practice, the layers are unidirectionally reinforced composites with the direction of fibers parallel to the x_1–x_2 plane. Let the fiber direction make an angle θ with the x_1-axis. A laminate is usually made of several such layers with different values of θ. Writing $x'_1 = x_1 \cos\theta + x_2 \sin\theta$, $x'_2 = -x_1 \sin\theta + x_2 \cos\theta$, a similar relationship between ξ'_j and ξ_j where ξ_j are the transform parameters introduced in eqn (4) and U'_i as the displacements in the x'_1, x'_2, x_3 directions one can express the transformed tractions at $z = h/2$ in the same directions in the following form for symmetric ($c = 1$) and antisymmetric ($c = 2$) displacement fields about the midplane of the layer

$$\overset{c}{\hat{\mathbf{T}}}(h/2) = \begin{bmatrix} \overset{c}{\tilde{\sigma}}'_{31}(h/2) \\ \overset{c}{\tilde{\sigma}}'_{32}(h/2) \\ \mathrm{i}\overset{c}{\tilde{\sigma}}'_{33}(h/2) \end{bmatrix} = \begin{bmatrix} \overset{c}{k}'_{11} & \overset{c}{k}'_{12} & \overset{c}{k}'_{13} \\ \text{sym.} & \overset{c}{k}'_{22} & \overset{c}{k}'_{23} \\ & & \overset{c}{k}'_{33} \end{bmatrix} \begin{bmatrix} \overset{c}{\tilde{u}}'_1(h/2) \\ \overset{c}{\tilde{u}}'_2(h/2) \\ \mathrm{i}\overset{c}{\tilde{u}}'_3(h/2) \end{bmatrix} = [\overset{c}{K}']\overset{c}{\tilde{\mathbf{U}}}'(h/2) \tag{A1}$$

where

$$\begin{aligned}
\overset{c}{\Delta}\overset{c}{k}'_{11} &= C_{55}[\lambda'_1\lambda'_2\lambda'_3(A^*_2 - A^*_1)f_1 f_2 + \xi'^2_2(A^*_1\lambda'^2_2 f_2 - A^*_2\lambda'^2_1 f_1)f_3] \\
\overset{c}{\Delta}\overset{c}{k}'_{12} &= C_{55}\xi'_1\xi'_2(\lambda'_2 f_2 - \lambda'_1 f_1)f_3 \\
\overset{c}{\Delta}\overset{c}{k}'_{13} &= C_{55}\xi'_1[-\lambda'_1\lambda'_3(1 - A^*_1)f_1 + \lambda'_2\lambda'_3(1 - A^*_2)f_2 - \xi'^2_2(A^*_1 - A^*_2)f_3] \\
\overset{c}{\Delta}\overset{c}{k}'_{22} &= C_{55}\xi'^2_1(A^*_2\lambda'^2_2 f_2 - A^*_1\lambda'^2_1 f_1)f_3 \\
\overset{c}{\Delta}\overset{c}{k}'_{23} &= C_{44}\xi'_2[2\lambda'_3(\lambda'_1 A^*_1 f_1 - \lambda'_2 A^*_2 f_2) - (\lambda'^2_3 + \xi'^2_2)(A^*_1 - A^*_2)f_3] \\
\overset{c}{\Delta}\overset{c}{k}'_{33} &= C_{55}\xi'^2_1\lambda'_3(A^*_2 - A^*_1)
\end{aligned}$$

and

$$\overset{c}{\Delta} = \lambda'_3(\lambda'_2 A^*_2 f_2 - \lambda'_1 A^*_1 f_1) + \xi'^2_2(A^*_1 - A^*_2)f_3 \tag{A2}$$

also f_q, $q = 1, 2, 3$ are given by

$$\begin{array}{lll} & \text{Case 1 } (c=1) & \text{Case 2 } (c=2) \\ f_q = & \tanh \lambda_q' \dfrac{h}{2} & \coth \lambda_q' \dfrac{h}{2} \end{array}$$

and

$$\begin{aligned} \kappa_q^2 &= \frac{1}{2}[\kappa' \pm \sqrt{(\kappa'^2 - 4C_{22}/C_{11})}], \quad q = 1,2 \\ A_q^* &= (C_{12}+C_{55})/(C_{55}-C_{22}/\kappa_q^2) \\ \kappa' &= (C_{11}C_{22}-C_{12}^2-2C_{12}C_{55})/C_{11}C_{55} \\ \kappa_3^2 &= C_{44}/C_{55} \\ \lambda_q' &= \sqrt{(\xi_1'^2/\kappa_q^2+\xi_2'^2)} \end{aligned} \tag{A3}$$

C_{ij} being the effective stiffness in contracted notations, direction 1 coinciding with the fiber direction and C_{55} and C_{44} denoting the axial and transverse shear moduli, respectively. Simple transformations can now be utilized to obtain the stiffness matrices used in eqn (5) from the elements of $[\overset{c}{K'}]$ given in eqn (A2). These transformations which include those to consider direction changes of in-plane displacements and shear tractions as well as the combination of symmetric and antisymmetric fields about $z = 0$ are omitted for brevity but can be found elsewhere[20].

APPENDIX B. TRANSFORMS OF TRACTIONS AT DISBONDED INTERFACES

Denoting the top and bottom surfaces of the laminate as the first and nth interface, respectively, and the lth interface ($1 < l < n$) as the one between the $(l-1)$th and lth layer we write $\mathbf{V}_l$ as the displacement vector at all perfectly bonded interfaces and at the first and nth interfaces. Note that

$$\mathbf{U}_1^l = \mathbf{U}_2^{l-1} = \mathbf{V}^l. \tag{B1}$$

At the disbonded interface l_j ($j = 1, 2, \ldots, m$) we introduce the unknowns V_{lj} such that

$$\bar{\mathbf{V}}_{l_j} = \bar{\mathbf{U}}_2^{l_j-1} - [K_{l_j}^0]\overset{11*}{[K_{l_j}]}\mathbf{V}_j^* \tag{B2}$$

where $\mathbf{V}_j^* = \mathbf{U}_2^{l_j-1} - \mathbf{U}_1^{l_j}$, is the displacement discontinuity.

$$\begin{aligned} &[K_{l_j}^0]^{-1} = \overset{11*}{[K_{l_j}]} + \overset{22*}{[K_{l_j-1}]} \\ &\overset{\alpha\beta*}{[K_{l_j}]} = \text{the asymptotic form of } \overset{\alpha\beta}{[K_{l_j}]} \text{ as } \xi \to \infty. \end{aligned} \tag{B3}$$

It follows that

$$\bar{\mathbf{U}}_1^{l_j} = \bar{\mathbf{V}}_{l_j} - [K_{l_j}^0]\overset{22*}{[K_{l_j-1}]}\bar{\mathbf{V}}_j^*. \tag{B4}$$

Substituting U_1^l, U_2^l from eqns (B1) to (B4) in eqn (5) and imposing the conditions that tractions $\mathbf{T}_1$, $\mathbf{T}_n$ are prescribed at the top and bottom surfaces and tractions at all other interfaces are self equilibrating (including the disbonded ones), i.e. $\mathbf{T}_1^l + \mathbf{T}_2^{l-1} = 0$, $1 < l < n$, one obtains

$$\underset{3n\times 3n}{[K^G]}\begin{bmatrix}\bar{\mathbf{V}}_1 \\ \bar{\mathbf{V}}_{l_j} \\ \bar{\mathbf{V}}_n\end{bmatrix} = \underset{3n\times 3m}{[B]}\begin{bmatrix}\bar{\mathbf{V}}_1^* \\ \vdots \\ \bar{\mathbf{V}}_j^* \\ \vdots \\ \bar{\mathbf{V}}_m^*\end{bmatrix} + \begin{bmatrix}\bar{\mathbf{T}}_1 \\ 0 \\ 0 \\ \vdots \\ \bar{\mathbf{T}}_n\end{bmatrix}. \tag{B5}$$

The matrix K^G is the global stiffness matrix in the transformed domain and the non-zero elements of columns $3j-2$, $3j-1$, and $3j$ of matrix B are given by

$$\begin{aligned} \text{Rows } 3l_j-5 \to 3l_j-3 \quad & -\overset{12}{[K_{l_j-1}]}[K_{l_j}^0]\overset{11*}{[K_{l_j}]} \\ \text{Rows } 3l_j-2 \to 3l_j \quad & \overset{11}{[K_{l_j}]}[K_{l_j}^0]\overset{22*}{[K_{l_j-1}]} - \overset{22}{[K_{l_j-1}]}[K_{l_j}^0]\overset{11*}{[K_{l_j}]} \\ \text{Rows } 3l_j+1 \to 3l_j+3 \quad & \overset{21}{[K_{l_j}]}[K_{l_j}^0]\overset{22*}{[K_{l_j-1}]}. \end{aligned} \tag{B6}$$

Equation (B5) can be formally solved to express $\bar{\mathbf{V}}_l$ as

$$\tilde{\mathbf{V}}_i = \sum_{p=1}^{m} [D_{lp}]\tilde{\mathbf{V}}_p^* + [E_{l1}]\tilde{\mathbf{T}}_1 + [E_{l2}]\tilde{\mathbf{T}}_n. \tag{B7}$$

The transform of the traction vector on the top face of layer l_j ($j = 1, 2, \ldots, m$) (corresponding to the bottom surface of disbonded interface l_j) can therefore be written (with the help of eqns (5), (B1)–(B4) and (B7)) as

$$\tilde{\mathbf{T}}_1^{l_j} = \tilde{\mathbf{T}}_j^* = [C^{*j}]\tilde{\mathbf{V}}_j^* + \sum_{p=1}^{m} [C^{jp}]\tilde{\mathbf{V}}_p^* + \tilde{\mathbf{T}}_j^0 \tag{B8}$$

where

$$[C_j^*] = -[\overset{11^*}{K}_{l_j}][K_{l_j}^0][\overset{22^*}{K}_{l_{j-1}}] \tag{B9}$$

$$[C^{jp}] = [\overset{11}{K}_{l_j}][D_{l_jp}] + [\overset{12}{K}_{l_j}][D_{(l_{j+1})p}] + [\overset{11^*}{K}_{l_j} - \overset{11}{K}_{l_j}][K_{l_j}^0][\overset{22^*}{K}_{l_{j-1}}]\delta_{jp} + [\overset{12}{K}_{l_j}][K_{l_{j+1}}^0][\overset{11^*}{K}_{l_{j+1}}]\delta_{(j+1)p}\,\delta_{(lj+1)l_{j+1}} \tag{B10}$$

δ_{jp} being the Kronecker delta. The term $\tilde{\mathbf{T}}_j^0$ is the contribution due to $\tilde{\mathbf{T}}_1$ and $\tilde{\mathbf{T}}_n$.

It should be noted that $[C^*]$ in eqn (B9) depends on the asymptotic forms $[\overset{11^*}{K}]$ and $[\overset{22^*}{K}]$ of $[\overset{11}{K}]$ and $[\overset{22}{K}]$ of the layers below and above the disbonded interface, respectively. Elements of these matrices can be obtained from those in Appendix A by substituting $f_1 = f_2 = f_3 = 1$ in eqn (A2) and performing the subsequent transformations. It can be shown that they are homogeneous functions of degree one in ξ_1, ξ_2 (the case of generally anisotropic half spaces with an interface flaw is discussed in Ref. [14]). If one now considers a single elliptic flaw with semiaxes a, a_2, and the principal axes coinciding with x_1, x_2 directions one can write

$$C_{k1}^*(\xi_1, \xi_2) = \xi C_{k1}^{**}\left(\frac{\xi_1}{\xi}, \frac{\xi_2}{\xi}\right) = \xi g(\phi) C_{k1}^{**}\left(\frac{\cos\phi}{a_1 g(\phi)}, \frac{\sin\phi}{a_2 g(\phi)}\right) \tag{B11}$$

where C^{**} also depends on the properties of the layers above and below the disbond

$$\xi_1 = \xi\frac{\cos\phi}{a_1}, \qquad \xi_2 = \xi\frac{\sin\phi}{a_2}$$

and g is given by eqn (20e).

The arguments of C_{k1}^{**} in eqn (B11) are the direction cosines of the normal to the ellipse at the point ($a_1\cos\phi$, $a_2\sin\phi$). Since the type of the stress-singularity at any point on the disbond periphery is characterized by the relative magnitudes of the elements of $[C^*]$ (see Ref. [14]) they depend only on the properties of the two layers and the direction of the normal to the ellipse at that point.

APPENDIX C: BONDED PLATE SOLUTIONS FOR MID-PLANE DISBONDS IN SYMMETRIC LAMINATES UNDER PLANE STRAIN CONDITIONS

Unit shear stress prescribed (Fig. 4)

In this case there is no deformation outside the region $-a \leqslant x \leqslant a$ and the in-plane displacement u_0, bending rotation ψ, axial force N and bending moment M in the top half are

$$u_0 = (a^2 - x^2)/2A, \qquad \psi = H(x^2 - a^2)/8D$$
$$N = -x, \qquad M = Hx/4 \tag{C1}$$

where A, D are the axial and bending of rigidity of the top (and bottom) half of the laminate and H is the total thickness (Fig. 4). For the bottom half ψ is of the same sign but N is the negative of that given by eqns (C1). There is a concentrated force of magnitude $t_c = a$ acting in the negative x direction. The gradient of the displacement discontinuity is given by $-4x(1/2A - H^2/32D)$.

Unit normal stress prescribed (Fig. 5)

This problem is symmetric about the mid-plane as well as $x = 0$ and for the top half we have $u_0 = N = 0$ everywhere. ψ, plate displacement gradient $w_{,x}$ and other stress resultants (Q being the shear force) are

For $\lvert x\rvert < a$	For $x > a$
$\psi = (-x^3/6 + M_0 x)/D$	$\psi = \psi(a)\,e^{-\lambda(x-a)}$
$w_{,x} = -(1/K + M_0/D)x + x^3/6D$	$w_{,x} = 0$
$Q = -x$	$Q = K\psi(a)\,e^{-\lambda(x-a)}$
$M = -x^2/2 + M_0$	$M = -\lambda D\psi(a)\,e^{-\lambda(x-a)}$

(C2)

where $\lambda^2 = K/D$, K being the shear stiffness of the top half. Unknown constants M_0 and $\psi(a)$ are evaluated from the conditions of continuity of ψ and M at $x = a$. The concentrated force on the top half in the z direction at the disbond tip is evaluated as the difference between values of Q for $x < a$ and $x > a$.

Energy release rates for both cases are computed as half of the product of the concentrated interactive force at the tip and the displacement discontinuity gradient[11, 13].